Volume 4, Number 2, 2011. pp. 59-69

Jordan Journal of Physics

REVIEW ARTICLE

Calculation of Thermoelectric Power and Electron Drift Mobility at Low Electric Field in $Al_xGa_{1-X}N$ Using an Iterative Method

Hadi Arabshahi

Department of Physics, Payame Nour University of Fariman, Fariman, Iran.

Received on: 21/12/2010; Accepted on: 10/1/2011

Abstract: An iteration calculation has been carried out to study electron transport properties in $Al_xGa_{1-x}N$ lattice-matched to GaN. The two-mode nature of the polar optic phonons is considered jointly with deformation potential acoustic, piezoelectric, ionized impurity and alloy scattering. Band non-parabolicity, admixture of *p*-functions, arbitrary degeneracy of the electron distribution and the screening effects of the free carriers on the scattering probabilities are incorporated. Electron drift mobility and thermoelectric power are calculated for different temperature and doping dependencies. It is found that the electron drift mobility decreases monotonically as the temperature increases from 100 K to 400 K. The low temperature value of electron mobility is also found to decreases significantly with increasing doping concentration. The agreement of iterative results with the available experimental data is found to be satisfactory.

Keywords: Iteration method; Thermoelectric power; Piezoelectric; Electron drift mobility.

1. Introduction

Gallium nitride has long been considered promising material for electronic and optoelectronic device applications [1-4]. The wide and direct energy gap, large breakdown field, high thermal conductivity and favorable electron-transport characteristics, make the GaN ideally suited for high-power and high-speed applications. While initial efforts to study this material were hindered by growth difficulties, recent improvements in the material quality have made the realization of a number of GaN-based devices possible. In particular, lasers [5], transistors and photodetectors [6] have been fabricated with these materials. These developments have fueled considerable interest in the GaN material.

In order to analyze and improve the design of GaN-based devices, an understanding of the electron transport that occurs within this material is necessary. While electron transport in bulk GaN has been extensively examined [7-9], the sensitivity of these results to variations in the material parameters has yet to be considered. Electron mobility in the ternary alloy has been measured; Monte Carlo calculations of mobility have also been performed [10]. In the mean time our knowledge of the basic parameters and of the scattering mechanisms for the alloy has improved. Particularly, it is now known that the polar-phonon scattering which is the dominant lattice scattering mechanism in the ternary alloy, has a two-mode character [11]. It is important to calculate the transport coefficients using such currently available information on scattering mechanisms and material parameters. We use such information in the present paper to calculate electron mobility and thermoelectric power in the $Al_xGa_{1-x}N$ alloy. We consider band non-parabolicity, admixture of *p*-type valence-band wave functions, degeneracy of the electron distribution to any arbitrary degree and the screening effects of free carriers on the scattering probabilities. Electrons in bulk material suffer intravalley scattering by polar optical, non-polar

Corresponding Author: Hadi Arabshahi. **Email**: arabshahi@um.ac.ir

optical, alloy, acoustic phonons, piezoelectric, plasmon and ionized impurity scattering.

Acoustic and piezoelectric scattering are assumed elastic and the absorption and emission rates are combined under the equipartition approximation which is valid for lattice temperatures above 77 K. Elastic ionized impurity scattering is described using the screened Coulomb potential of the Brooks-Herring model [12]. The Boltzmann equation is solved iteratively for our purpose, jointly incorporating the effects of all the scattering mechanisms. Our calculated results are compared with the available experimental data on both the temperature and the compensation dependence of mobility.

This paper is organized as follows. Details of the iterative model and the electron mobility and thermoelectric power calculations are presented in section 2 and the results of iterative calculations carried out on $Al_xGa_{1-x}N$ structures are interpreted in section 3 and finally conclusions are drawn in section 4.

2. Theoretical model

In principle the iterative technique gives exact numerical prediction of electron mobility in bulk semiconductors. To calculate mobility, we have to solve the Boltzmann equation to get the modified probability distribution function under the action of a steady electric field. Here, we have adopted the iterative technique for solving the Boltzmann transport equation. Under application of a uniform electric field the Boltzmann equation can be written as

$$(\frac{e}{\hbar})E.\nabla_k f = \oint [s'f'(1-f)-sf(1-f')]\,dk \qquad (1)$$

where $f = f(k)$ and $f' = f(k')$ are the probability distribution functions and $s = s(k,k')$ and $s' = s(k',k)$ are the differential scattering rates. If the electric field is small, we can treat the change from the equilibrium distribution function as a perturbation which is first order in the electric field. The distribution in the presence of a sufficiently small field can be written quite generally as

$$f(k) = f_0(k) + g(k)\cos\theta \qquad (2)$$

where, $f_0(k)$ is the equilibrium distribution function, θ is the angle between k and E and $g(k)$ is an isotropic function of k, which is proportional to the magnitude of the electric field. In general, contributions to the differential scattering rates come from two types of scattering processes, elastic scattering, s_{el}, due to acoustic, impurity, plasmon and piezoelectric phonons, and inelastic scattering, s_{inel}, due to polar optic phonons

$$s(k,k') = s_{el}(k,k') + s_{inel}(k,k') \qquad (3)$$

The polar phonon energy is quite high (~92 mev) in case of GaN. Hence, this scattering process cannot be treated within the framework of the relaxation time approximation (RTA) because of the possibility of the significant energy exchange between the electron and the polar optic modes. In this case, s_{inel} represents transitions from the state characterized by k to k, either by emission $[s_{em}(k,k')]$ or by absorption $[s_{ab}(k,k')]$ of a phonon. The total elastic scattering rate will be the sum of all the different scattering rates which are considered as elastic processes, i.e. acoustic, piezoelectric, ionized impurity, and electron-plasmon scattering. In the case of polar optic phonon scattering, we have to consider scattering-in rates by phonon emission and absorption as well as scattering-out rates by phonon absorption and emission. Using Boltzmann equation and considering all differential scattering rates, the factor $g(k)$ in the perturbed part of the distribution function $f(k)$ can be given by

$$g(k) = \frac{\frac{-eE}{\hbar}\frac{\partial f_0}{\partial k} + \sum\int g'\cos\varphi[s_{inel}'(1-f) + s_{inel}f]dk}{\sum\int(1-\cos\varphi)s_{el}dk + \sum\int[s_{inel}(1-f') + s_{inel}'f']dk} \qquad (4)$$

Note, the first term in the denominator is simply the momentum relaxation rate for elastic scattering. It is interesting to note that if the initial distribution is chosen to be the equilibrium distribution, for which $g(k)$ is equal to zero, we get the relaxation time approximation result after the first iteration. We have found that convergence can normally be achieved after only a few iterations for small electric fields. Once $g(k)$ has been evaluated to the required accuracy, it is possible to calculate quantities such as the drift mobility which is given by

$$\mu_d = \frac{\hbar}{3m} \frac{\int_0^\infty k^3 \frac{g(k)}{Ed} dk}{\int_0^\infty k^2 f(k) dk} \tag{5}$$

where d is defined as $1/d = m\nabla_k E/\hbar^2 k$. Here, we have calculated low field drift mobility in $Al_xGa_{1-x}N$ structure using the iterative technique. In the following sections electron-phonon, electron-impurity, electron-plasmon and alloy scattering mechanisms will be discussed.

A. Deformation potential scattering

The acoustic modes modulate the inter-atomic spacing. Consequently, the position of the conduction and valence band edges and the energy band gap will vary with position because of the sensitivity of the band structure to the lattice spacing. The energy change of a band edge due to this mechanism is defined by a deformation potential and the resultant scattering of carriers is called deformation potential scattering. The energy range involved in the case of scattering by acoustic phonons is from zero to $2\hbar v_s k$, where v_s is the velocity of sound, since momentum conservation restricts the change of phonon wave-vector to between zero and $2k$, where k is the electron wave-vector. Typically, the average value of k is of the order of 10^7 cm^{-1} and the velocity of sound in the medium, is of the order of 10^5 cms^{-1}. Hence, $2\hbar v_s k \sim 1$ meV, which is small compared to the thermal energy at room temperature. Therefore, the deformation potential scattering by acoustic modes can be considered as an elastic process except at very low temperature. The deformation potential scattering rate with either phonon emission or absorption for an electron of energy E in a non-parabolic band is given by Fermi's golden rule as [13-14]

$$\left.\begin{aligned} S_{ac}(k,k') = \frac{\sqrt{2}D_{ac}^2 (m_t^* m_l^*)^{1/2} K_B T}{\pi\rho v^2 \hbar^4} \times \\ \frac{\sqrt{E(1+\alpha E)}}{(1+2\alpha E)}[(1+\alpha E)^2 + 1/3(\alpha E)^2] \end{aligned}\right\} \tag{6}$$

where D_{ac} is the acoustic deformation potential, ρ is the material density and α is the non-parabolicity coefficient. This formula clearly shows that the acoustic scattering increases with temperature.

B. Piezoelectric scattering

The second type of electron scattering by acoustic modes occurs when the displacements of the atoms create an electric field through the piezoelectric effect. This can occur in the compound semiconductors such as the III-V and II-VI materials including GaN, which in fact has a relatively large piezoelectric constant. The piezoelectric scattering rate for an electron of energy E in an isotropic, parabolic band has been discussed by Ridley [15] who included the modification of the Coulomb potential due to free carrier screening. The screened Coulomb potential is written as

$$V(r) = \frac{e^2}{4\pi\varepsilon_0\varepsilon_s} . \frac{\exp(-q_0 r)}{r} \tag{7}$$

where ε_s is the relative dielectric constant of the material and q_0 is the inverse screening length, which under non-degenerate conditions is given by

$$q_0^2 = \frac{ne^2}{\varepsilon_0 \varepsilon_s k_B T} \tag{8}$$

where n is the electron density. The expression for the scattering rate of an electron in a non-parabolic band structure retaining only the important terms can be written as [13-14]

$$\begin{aligned} R_{pz}(k) = \frac{\sqrt{m^*} e^2 K_{av}^2 K_B T}{4\sqrt{2}\pi\hbar^2 \varepsilon_0 \varepsilon_s} \gamma^{-1/2}(E)(1+2\alpha E)^2 \times \\ \left[\ln(1 + \frac{8m^*\gamma(E)}{\hbar^2 q_0^2} - \frac{1}{1+\hbar^2 q_0^2/8m^*\gamma(E)} + \left(\frac{\sqrt{2}\alpha E}{1+2\alpha E}\right)^2 \right] \end{aligned} \tag{9}$$

where K_{ac} is the dimensionless so called average electromechanical coupling constant.

C. Polar optical phonon scattering

The dipolar electric field arising from the opposite displacement of the negatively and positively charged atoms provides a coupling between the electrons and the lattice which results in electron scattering. This type of scattering is called polar optical phonon scattering and at room temperature is generally the most important scattering mechanism for electrons in III-V semiconductors. This is also the case in GaN despite the fact that the optical phonon energy is particularly high at ~92 meV which suppresses the phonon population and also electrons must reach that energy before phonon emission is possible. The scattering rate due to this process for an electron of energy E in an isotropic, non-parabolic band is [13-14]

$$\left.\begin{array}{l} R_{po}(k) = \dfrac{\sqrt{2m^*}e^2\omega_{op}}{8\pi\varepsilon_0\hbar}\left(\dfrac{1}{\varepsilon_\infty}-\dfrac{1}{\varepsilon_s}\right)\dfrac{1+2\alpha E'}{\gamma^{1/2}(E)} \\ \times F_0(E,E')\left\{N_{op},N_{op}+1\right\} \end{array}\right\} \qquad (10)$$

where

$$\left.\begin{array}{l} F_0(E,E') = C^{-1}\left\{A\ln\left|\dfrac{\gamma(E)^{1/2}+\gamma(E')^{1/2}}{\gamma(E)^{1/2}-\gamma(E')^{1/2}}\right|+B\right\} \\ A = \left[2(1+\alpha E)(1+\alpha E')+\alpha(\gamma+\gamma')\right]^2 \\ B = -2\alpha\gamma^{1/2}\gamma'^{1/2}\left[4(1+\alpha E)(1+\alpha E')+\alpha(\gamma+\gamma')\right] \\ C = 4(1+\alpha E)(1+\alpha E')(1+2\alpha E)(1+2\alpha E') \end{array}\right\} \qquad (11)$$

where N_{op} is the phonon occupation number and the upper and lower cases refer to absorption and emission, respectively. For small electric fields, the phonon population will be very close to equilibrium so that the average number of phonons is given by the Bose-Einstein distribution

$$N_{op} = \frac{1}{\exp\left(\dfrac{\hbar\omega_{op}}{K_BT}\right)-1} \qquad (12)$$

where $\hbar\omega_{op}$ is the polar optical phonon energy.

D. Non-polar optical phonon scattering

Non-polar optical phonon scattering is similar to deformation potential scattering, in that the deformation of the lattice produces a perturbing potential but in this case the deformation is carried by optical vibrations. The non-polar optical phonon scattering rate in non-parabolic bands is given by [13-14]

$$R_{npo}(k) = \frac{D_{od}^2(m_t^{*2}m_l^*)^{1/2}}{\sqrt{2}\pi\hbar^3\rho\omega_{op}}(1+2\alpha E)\gamma^{1/2}(E)\left[N_{op},N_{op}+1\right] \quad (13)$$

where D_{od} is the optical deformation potential and $E = E'\pm\hbar\omega_{op}$ is the final state energy phonon absorption (upper case) and emission (lower case).

E. Intravalley impurity scattering

The standard technique for dealing with ionized impurity scattering in semiconductors is the Brook-Herring (BH) technique [15], which is based on two inherent approximations. First, is the first order Born approximation and second is the single ion screening approximation. These two approximations essentially lead to a poor fit to the experimental mobility data [16]. Several attempts have been made to modify the BH technique phenomenologically [17]. It has been shown that phase-shift analysis of electron-impurity scattering is the best way to overcome the Born approximation. Departure from the BH predictions of electron mobility is evident at higher electron concentrations. Meyer and Bartoli [18-19] have provided an analytic treatment based on phase-shift analysis taking into account the multi-ion screening effect and finally been able to overcome both the approximations. All the previous techniques of impurity screening by free electrons in semiconductors were based on the Thomas-Fermi (TF) approximation which assures that a given impurity should be fully screened. The breakdown of the single-ion screening formalism becomes prominent in the strong screening regime, where the screening length calculated through TF theory becomes much shorter than the average distance between the impurities and hence neighboring potentials do not overlap significantly. This essentially leads to a physically unreasonable result. In the case of high compensation, the single-ion screening formalism becomes less relevant, because in order to maintain the charge neutrality condition, it would be more difficult for a given number of electrons to screen all the ionized donors separately. In the case of GaN, the compensation ratio is usually quite large, and the ratio N_D^+/n is also temperature dependent. Hence the multi-ion screening correction is very essential in GaN. The effective potential of an ionized impurity scattering center is spherically symmetric in nature, so one can use phase-shift analysis to find the differential scattering rate $s(k,k')$ more accurately. The effective potential $V(r)$ due to an ionized impurity can be expressed as: $V(r)=-(Z_l e^2)/(4\pi\varepsilon_0\kappa_0 r)e^{-r/\lambda}$, where Z_l is the charge of the ionized impurity in units of e and λ is the screening length. The standard technique to find out the screening length is the TF approach which is based on single ion screening approximation. In TF one can calculate the charge contribution q_i to the screening of a single ionized donor by an electron of energy E_i and is given by $q_i=-(2e^3\lambda^2/\varepsilon_0\kappa_0 E_i V)$. In the case of multi-ion problem, the TF approach can be generalized to find out the effective charge contribution due to an electron to screen all ionized donors and can be given by: $Q_i=-(2e^3N_D^+\lambda^2/\varepsilon_0\kappa_0 E_i)$. Total screening charge exactly neutralizes the ionized donors, when Q_i is summed over all electronic states

$$\sum_i -\frac{Q_i}{e} f_0(E_i)=N_D^+ \tag{14}$$

For the sufficiently low energy electrons, Q_i can be greater than the electronic charge, which is physically unreasonable. One way to tackle this problem is to introduce a factor S_i such that

$$S_i(E_i)=\frac{E_i}{\xi} \tag{15}$$

where $\xi=(2N_D^+c^2\lambda^2/\varepsilon_0 k_0)$, Q_i will be modified to $Q_i^{'}=Q_iS_i$ in equation 14. For the low energy electrons the contribution will be –e. Since the total contribution to the screening by the low energy electrons has been effectively decreased, equation 14 no longer holds. However, if the screening length λ is more than the average distance between the donors, it is not necessary to insist that each donor be fully screened, only it is required that overall charge neutrality should be preserved. Electrons in the overlap region can provide screening to both the ionized donors. Here we can define a factor p, which would be the fraction of the total charge, which is contained within a sphere of radius R surrounding the donor. Hence equation 14 will be modified as

$$\sum_i -\frac{Q_i^{''}}{e} f_0(E_i)=pN_D^+ \tag{16}$$

where $Q_i^{''}=p\,Q_i\,S_i$. The screening charge requirement will be fulfilled by adjusting the screening length until equation 16 is satisfied and is given by:

$$\lambda_m^{-2}=\eta\lambda_0^{-2} \tag{17}$$

where λ_m is multi-ion screening length and λ_0 is TF screening length. The differential scattering rate for ionized impurity can be given as

$$S_{ii}(k,k')=\frac{8\pi^3\hbar^3}{m^{*2}V^2}\left|f(X)\right|^2\delta[E(k')-E(k)] \tag{18}$$

Where the scattering amplitude $f(X)$ depends on the phase shift δ_l and Legendre polynomial P_l and is given by

$$f(X)=\frac{1}{2ik}\sum_{l=0}^{\infty}(2l+1)(e^{2i\delta_l}-1)P_l(X) \tag{19}$$

It has already been mentioned that in n-type GaN the activation energy of the donors is quite large, which keeps a large number of donors neutral at low temperatures. Neutral impurity scattering has been dealt with previously using the Erginsoy expression [20] which is based on electron scattering by a hydrogen atom and a scaling of the material parameters. It has been shown that an error as high as 45% results in the neutral impurity scattering cross section with this simple model. Meyer and Bartoli [18-19] have given a phase shift analysis treatment based on the variation results of Schwartz [21] to calculate the neutral impurity cross section, which is applicable for a larger range of electron energy.

F. Intravalley alloy scattering

Alloy scattering refers to the scattering due to the random distribution of the component atoms of the alloy among the available lattice sites. Harrison *et al.* [22] assumed that the alloy crystal potential can be described as a perfectly periodic potential which is then perturbed by the local deviations from this potential, due to the disordering effects in the alloy. Using the Harrison model [22], the scattering rate due to the chemical disorder in a ternary alloy of electrons in a non-parabolic band is given by [13-14]

$$\left.\begin{aligned} R_{alloy}(k) &= \frac{4\sqrt{2}\pi m^{*3/2}r_0^6}{9\hbar^4}\,\frac{x(1-x)(\Delta U)^2}{\Omega^2} \\ &\times\ \gamma^{1/2}(E)(1+2\alpha E) \end{aligned}\right\} \tag{20}$$

where x denotes the molar fraction of one of the binary components of the alloy, Ω is the volume of the primitive cell and ΔU is the spherical scattering potential.

G. Intravalley scattering due to optical phonons

The constant energy surfaces for the conduction band of GaN derive from several valleys. Thus, under the application of high electric field, electrons can be scattered from an initial state in a certain valley to a final state in a non-equivalent valley. For example, in wurtzite GaN this process occurs when an electron in the Γ valley is heated and is able to transfer to the higher *U* and *K* valleys. In the case of Γ to zone edge valley scattering the process involves a substantial change of electron wave-vector. Acoustic and optical phonons of sufficiently large wave-vector can effect the transition but in view of the large wave-vectors involved it is normal to treat all processes like deformation scattering by optical phonons. Then the total nonequivalent intervalley scattering rate from a state *k* in a certain valley to a set of Z_f different valleys is given by [13-14]

$$R_{equiv}(k)=\frac{(D_tK)_i^2 Z_f (m_t^{*2}m_l^*)^{1/2}}{\sqrt{2}\pi\rho\omega_{op}\hbar^3}(\varepsilon\pm\hbar\omega_{op}-\Delta\varepsilon_{fi})^{1/2}\times\left[1+2\alpha(\varepsilon\pm\hbar\omega_{op}-\Delta\varepsilon_{fi})\right]\left\{N_{op,}N_{op}+1\right\} \tag{21}$$

where $\hbar\omega_{op}$ is the optical phonon energy and $\Delta\varepsilon_{fi}$ is the difference between the energies of the bottoms of the final and initial valleys. $(D_tK)_i$ is the coupling constant, which depends on the initial and final valleys and the branch of phonons involved in the transition. N_{op} is the phonon occupation number, with the upper and lower cases corresponding to phonon absorption and emission, respectively.

H. Electron-plasmon scattering

The electron-plasmon interaction Hamiltonian can be written in random phase approximation as [23]

$$H_{\text{int}}=\sum M_q(a_q c_{k+q}^+ c_k + a_{-q}^+ c_{k+q}^+ c_k) \tag{22}$$

Here a_q^+, a_q and c_k^+, c_k are the creation and annihilation operators for plasmons and electrons, respectively. The matrix element

$$M_q=\sqrt{\frac{e^2\hbar^3}{8\Omega\varepsilon m^{*2}\omega_p(q)}}.(2qk+q^2)/q \tag{23}$$

where $\omega_p(q)$ is the dispersion relation for plasmons, *q* and *k* are the plasmon and electron momenta, respectively, *e* and *m** are the charge and effective mass of an electron, ε the background dielectric constant, and Ω the real-space volume. The first term in parentheses in equation 22 describes the plasmon absorption process which obeys the energy conservation law as

$$\varepsilon_{k+q}-\varepsilon_k=\hbar\omega_p(q)\geq 0 \tag{24}$$

where ε_k is the energy of electron with momentum *k*. In a similar manner, the plasmon emission process, in accordance with the second term in parentheses in equation 22, is governed by the energy conservation law which can be written as

$$\varepsilon_k-\varepsilon_{k+q}=\hbar\omega_p(q)\geq 0 \tag{25}$$

Note that equation 24 describes the emission of plasmon with momentum -*q*. To impart a more conventional form to the energy conservation law, replace the variable of summation *q* in terms governing the plasmon emission in equation 1 by -*q*. Then we can rewrite equation 22 as

$$H_{\text{int}}=\sum(M_q a_q c_{k+q}^+ c_k + M_{-q} a_q^+ c_{k-q}^+ c_k) \tag{26}$$

The notation of equation 22 leads to the following form of the energy conservation law for the emission processes

$$\varepsilon_k-\varepsilon_{k-q}=\hbar\omega_p(q)\geq 0 \tag{27}$$

From the Fermi Golden rule, we can calculate the electron-plasmon scattering rates for emission W_e and absorption W_a

$$\left.\begin{aligned} W_{e,a}(k) &= \frac{2\pi}{\hbar}\int\frac{\Omega dq}{8\pi^3}\left|\langle f|H_{\text{int}}|i\rangle\right|^2 \\ &\times\delta\left[\varepsilon_{k'}-\varepsilon_k\pm\hbar\omega_p(q)\right]\end{aligned}\right\} \tag{28}$$

where *k* and *k*' are electron momenta in an initial state $|i\rangle$ and a final state $|f\rangle$, respectively. Here and further the upper signs in formulae correspond to the plasmon emission, whereas the lower ones do to the plasmon absorption. By using equation 22 and the energy conservation requirements in the forms of equations 24 and 26 which are consistent with this notation of H_{int}, equation 28 becomes

$$W_{e,a}(k) = \frac{2\pi}{\hbar}\int \frac{\Omega dq}{8\pi^3} M^2_{\mp q}\,\delta\left[\varepsilon_{k\mp q} - \varepsilon_k \pm \hbar\omega_p(q)\right] \times \left\{(N_q+1)_{em};(N_q)_{ab}\right\} \tag{29}$$

where N_q is the Bose-Einstein distribution function for plasmons. The integration bounds with respect to q are defined from the following conditions

$$\left.\begin{aligned} \omega_p(q) &\le \hbar k q/m^* \mp \hbar q^2/2m^* \\ \omega_p(q) &\ge \hbar k_f q/m^* + \hbar q^2/2m^* \end{aligned}\right\} \tag{30}$$

where k_f is the electron momentum at the Fermi surface.

I. Thermoelectric power

The thermoelectric power Q, is the ratio of electric field E to temperature gradient ∇T across an open-circuited crystal, i.e., the electron current density J is set equal to zero. Theoretically, the current density in the presence of electric field E and temperature gradient ∇T in an isotropic crystal is

$$J = \sigma[E - (\nabla E_F/e) - Q] \tag{31}$$

where σ is the conductivity and E_F is the Fermi energy. Equation 31 is valid for the small driving forces considered here, for which σ and Q are independent of the field strengths. When $J = 0$, as in the open-circuit measurement of Q, the crystal maintains equilibrium so that $\nabla E_F = 0$ and

$$Q = E/(\partial T/\partial z) \tag{32}$$

which is the defining equation for Q. The temperature gradient is taken parallel to the z-axis. Since all driving forces are small, the transport coefficients σ and Q are constant and equation 32 yields Q also in the short-circuit case when $E = 0$

$$Q = \left[\frac{\partial E_F}{\partial z}/e + \frac{J}{\sigma}\right] / \frac{\partial T}{\partial z} \tag{33}$$

Substitution Poisson's equation and Fermi-Dirac distribution function in equation 33, the thermoelectric power is

$$Q = \frac{k}{e}\left[\frac{\int k^2 f(1-f)(E/T)dk}{\int k^2 f(1-f)dk} - \frac{E_F}{kT}\right] - \frac{J/\sigma}{\partial T/\partial z} \tag{34}$$

Important parameters used throughout the simulations are listed in Table 1.

Table 1: Valley and material parameters of energy band structure for wurtzite structure of GaN and $Al_{0.2}Ga_{0.8}N$ used in the present model [5-11].

	GaN	$Al_{0.2}Ga_{0.8}N$
Density ρ (kgm^{-3})	6150	6810
Longitudinal sound velocity v_s (ms^{-1})	6560	6240
Low-frequency dielectric constant ε_s	9.5	15.3
High-frequency dielectric constant ε_∞	5.35	8.4
Acoustic deformation potential (eV)	8.3	7.1
Polar optical phonon energy (eV)	0.0995	0.089
Γ-valley effective mass (m*)	0.2	0.11
U-valley effective mass (m*)	0.4	0.4
K–valley effective mass (m*)	0.3	0.3
Γ-valley nonparabolicity (eV^{-1})	0.189	0.419
U-valley nonparabolicity (eV^{-1})	0.065	0.065
K-valley nonparabolicity (eV^{-1})	0.7	0.7

3. Calculation results

Low field electron mobility in $Al_xGa_{1-x}N$ as a function of temperature and doping concentration has been performed by Morkoc [24] and Udayan *et al.* [25]. Their calculations show that an electron mobility as high as 900 $cm^2V^{-1}s^{-1}$ could be achieved in case of uncompensated $Al_xGa_{1-x}N$ at room temperature. In the case of high quality samples with very low compensation, a mobility of more than 800 $cm^2V^{-1}s^{-1}$, at room temperature, with a similar doping concentration has been reported. On the other hand, there has been very little work on the calculation of low field electron mobility in $Al_xGa_{1-x}N$. Wang *et al.* [26] have used the variational principle to calculate low field electron mobilities and compared their results with fairly old experimental data. They have tried to fit the experimental data with an overestimated compensation ratio. In old samples, low electron mobility was due to poor substrate and buffer quality and other growth related problems. The iterative technique has been used by Rode and Gaskill [2] for low field electron mobility in GaN for the dependence of mobility on electron concentration, but not on temperature, and ionized impurity scattering has been estimated within the Born approximation, which might be the reason for poor fitting at high electron concentrations.

Here we have performed a series of low-field electron mobility calculations in $Al_xGa_{1-x}N$ structure. Low field mobilities have been derived using iteration method. Fig. 1 shows the temperature dependence of electron drift mobility in $Al_xGa_{1-x}N$ for $x = 0.2$, 0.4 and 0.5. In curve 1, the carrier concentration is taken to be $n = 10^{17}$ cm^{-3}. The ionized impurity concentration is put equal to the electron concentration. In curve 2, n is taken to be $n = 5\times10^{17}$ cm^{-3} and in curve 3, n is given the value of 10^{18} cm^{-3}. The results plotted in figure 1 indicate that the electron drift mobility decrease with increasing temperature due to increasing optical phonon scattering rate. Also it can be seen that with increasing compensation from 0.2 to 0.5 the calculated electron drift mobility is decreased due to a higher impurity scattering rate. This is also largely due to the higher Γ valley effective mass in the higher compensation ratio.

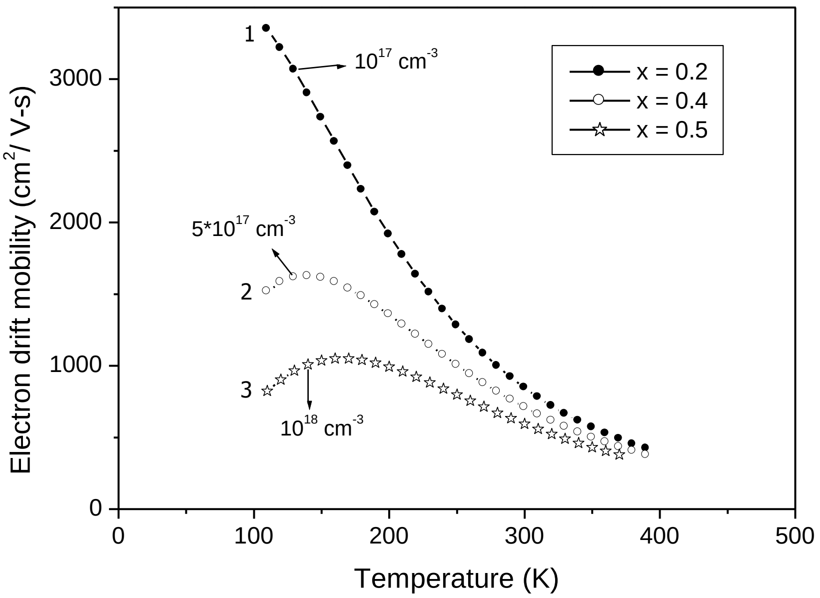

FIG.1. Variation of electron drift mobility with temperature for $Al_xGa_{1-x}N$ lattice-matched to GaN, for $x = 0.2$ (curve 1), $x = 0.4$ (curve 2) and $x = 0.5$ (curve 3). In curve 1, $n = 10^{17}$ cm^{-3}, in curve 2, $n = 5\times10^{17} cm^{-3}$ and in curve 3, $n = 10^{18}$ cm^{-3}.

Fig. 2 shows the calculated variation of the electron mobility as a function of the donor concentration for different compensation ratio. The mobility does not vary monotonically between donor concentrations of 10^{17} and 10^{18} cm^{-3} due to the dependence of electron scattering on donor concentration, but reaches to a value of 850 and 550 $cm^2V^{-1}s^{-1}$ for donor concentrations of 10^{17} and 10^{18} cm^{-3}, respectively.

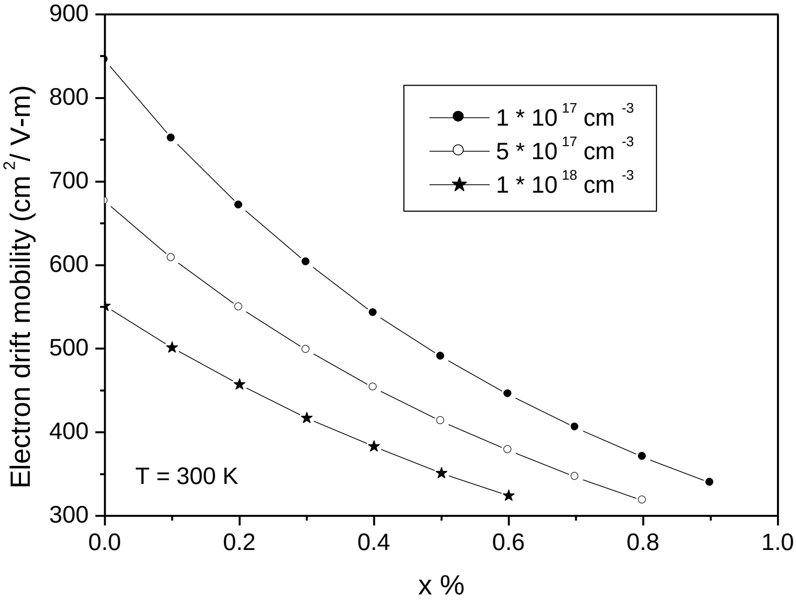

FIG.2. Variation of electron drift mobility with different compensation ratio for $Al_xGa_{1-x}N$ lattice-matched to GaN at room temperature. Calculated curves are for $n = 10^{17}$ cm^{-3}, $n = 5\times10^{17}$cm^{-3} and $n = 10^{18}$ cm^{-3}.

In order to understand the scattering mechanisms which limit the mobility of $Al_xGa_{1-x}N$ under various conditions, we have performed calculations of the electron drift mobility when particular scattering processes are ignored. The solid curve in Fig. 3 shows the calculated mobility for including all scattering mechanisms whereas the dashed, dotted, and open circle curves show the calculated mobility without ionized impurity, piezoelectric and polar optical scattering, respectively. It can be seen that below 300 K the ionized impurity scattering is dominant while at the higher temperatures electron scattering is predominantly by optical modes.

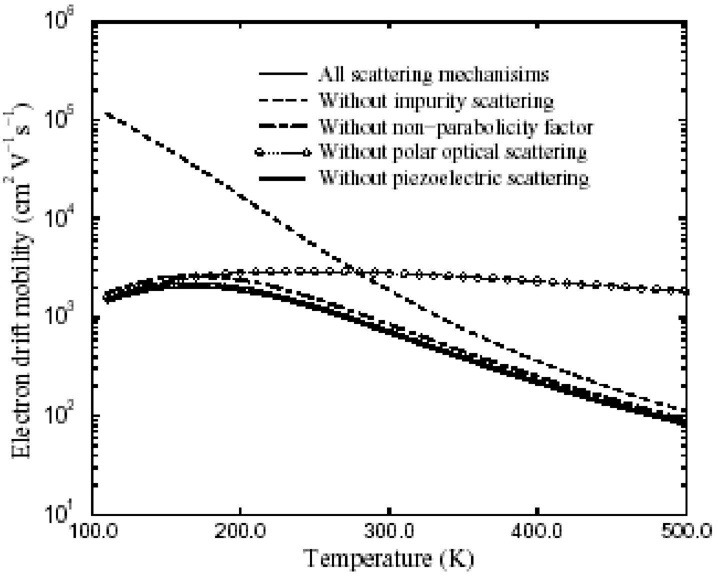

FIG.3. Comparison of electron drift mobility in wurtzite $Al_xGa_{1-x}N$ with donor concentration of $n = 10^{17}$ cm^{-3} and when individual scattering processes are ignored. The effect of Γ-valley non-parabolicity is also shown.

Thus the marked reduction in mobility at low temperatures seen in Fig. 3 can be ascribed to impurity scattering and that at high temperatures to polar optical phonon scattering. In figure 3 the mobility in the absence of band non-parabolicity is plotted as a dash-dot curve. Non-parabolicity leads to approximately a 8% reduction relative to the mobility for parabolic band at room temperature. This is because non-parabolicity increases the electron effective mass and also the scattering rates through the density of states.

The temperature variation of thermoelectric power Q for $x = 0.2$ is shown in Fig. 4. The magnitude of Q increases with temperature mainly because the material becomes more non-degenerate with a rise in temperature. Also, assuming that the material is uncompensated, the thermoelectric power for $n = 10^{18}$ (curve 3) is larger in magnitude than for $n = 10^{17}$ (curve 1) since the Fermi level is higher in the latter case. Considering curves 1 and 3, we find that the magnitude of Q for a compensated sample is larger. This is due to the enhancement of ionized impurity scattering.

The room temperature values of Q for an uncompensated material are plotted as a function of x in figure 5. The effective mass decreases with x, causing an upward movement of the Fermi level with a rise in x. This results in the decrease of Q with increasing x. It is clear from Fig. 5 that inclusion of ionized impurity scattering enhances Q while that of alloy scattering reduces Q. Our calculated results on thermoelectric power could not be compared with experiments since no such data could be traced in the literature.

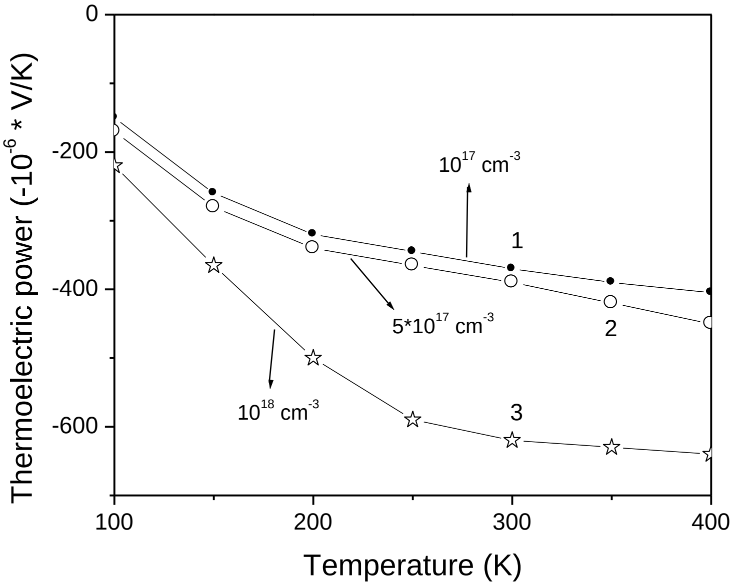

FIG.4. Temperature dependence of thermoelectric power of $Al_xGa_{1-x}N$ lattice-matched to GaN for $x = 0.2$. In curve 1, $n = 10^{17}$, in curve 2, 5×10^{17} and in curve 3, $n = 10^{18}$ cm^{-3}.

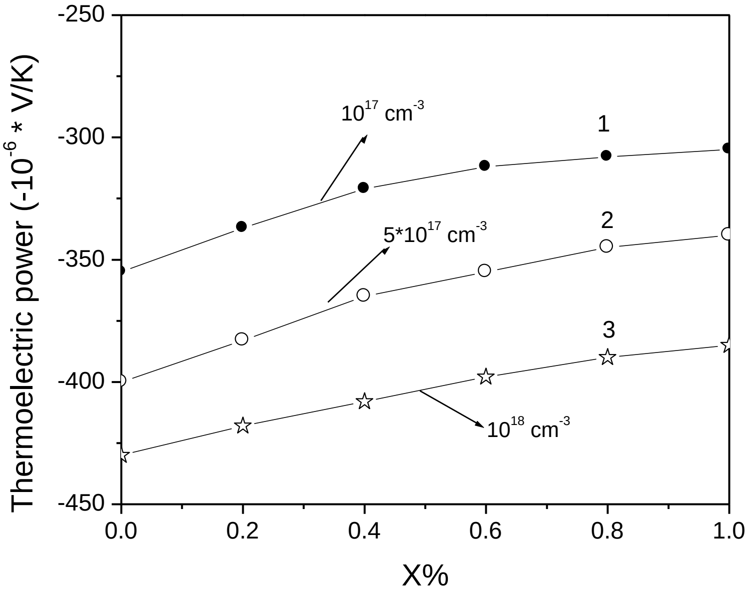

FIG.5. Compensation dependence of room temperature values of thermoelectric power of $Al_xGa_{1-x}N$ lattice-matched to GaN. In curve 1, $n = 10^{17}$, in curve 2, 5×10^{17} and in curve 3, $n = 10^{18}$ cm^{-3}.

4. Conclusions

In conclusion, we have studied the electron transport characteristic associated with wurtzite $Al_xGa_{1-x}N$ lattice-matched to GaN. Temperature dependent and free electron concentration dependent of the electron drift mobility have been calculated. It has been found that the low-field electron mobility is significantly higher for the $Al_xGa_{1-x}N$ structure with lower compensation ratio due to the lower Γ electron effective mass. Several scattering mechanisms have been included in the calculation. Ionized impurities have been treated beyond the Born approximation using a phase shift analysis. Screening of ionized impurities has been treated more realistically using a multi-ion screening formalism, which is more relevant in the case of highly compensated III-V semiconductors like GaN.

References

[1]Chin, V.W.L. and Tansley, T. L., J. Appl. Phys. 75 (1994) 7365.

[2]Rode, D.L. and Gaskill, D.K., Appl. Phys. Lett. 66 (1995) 1972.

[3]Tsen, K.T., Ferry, D.K., Botchkarev, A., Suerd, B., Salvador, A. and Morkoc, H., Appl. Phys. Lett. 71 (1997) 1852.

[4]Arabshahi, H. and Abadi, M.R.R., Brazilian Journal of Physics, 40(3) (2010) 267.

[5]Arabshahi, H. and Gholafroz, S., International Journal of the Physical science, 5(6) (2010) 690.

[6]Arabshahi, H., Turk. J. Phys. 33 (2009) 217.

[7]Arabshahi, H., Modern Physics Letters B, 23(8) (2009) 1101.

[8]Arabshahi, H. and Mowlavi, A.A., Modern Physics Letters B, 23(10) (2009) 1359.

[9]Arabshahi, H., Abadi, M.R.R. and Badieyan, F., Maejo Int. J. of Sci. Technol. 4(1) (2009) 159.

[10]Arabshahi, H., Benam, M.R. and Salahi, B. Modern Physics Letters B, 21 (2007) 1715.

[11]Arabshahi, H., Modern Physics Letters B, 21 (2007) 199.

[12]Brooks, H., Phys. Rev. 83 (1951) 879.

[13]Moglestue, C., Monte Carlo simulation of semiconductor devices, (Chapman and Hall, 1993).

[14]Jacoboni, C. and Lugli, P., The Monte Carlo Method for semiconductor and Device Simulation, (Springer-Verlag., 1989) p.87-112.

[15]Ridley, B.K., Electrons and phonons in semiconductor multilayers, (Cambridge University press, 1997).

[16]Di, K. and Brennan, K., J. Appl. Phys. 69 (1991) 3097.

[17]Mansour, N., Di, K. and Brennan, K., J. Appl. Phys. 70 (1991) 6854.

[18]Meyer, J.R. and Bartoli, F.J., Phys. Rev. B, 23 (1981) 5413.

[19]Meyer, J.R. and Bartoli, F.J., Solid State State Commun. 41 (1982) 19.

[20]Erginsoy, C., Phys. Rev. 79 (1950) 1013.

[21]Schwartz, C., Phys. Rev. 124 (1961) 1468.

[22]Harrison, J.W. and Hauser, J.R., Phys. Rev. B, 13 (1976) 5347.

[23]Chattopadhya, D. and Queisser, H.J., Rev. Mod. Phys. 53 (1981) 745.

[24]Morkoc, H., Nitride semiconductor and devices, (Springer-velag, 1999).

[25]Udayan, Bhapkar, V. and Shur, M.S., J. Appl. Phys. 82 (1997) 1649.

[26]Wang, R.P., Ruden, P.P., Kolnik, J. and Brennan, K.F., Mat. Res. Soc. Symp. Proc. 445 (1997) 935.